NASA Technical Memorandum 104424

An Efficient and Robust Algorithm for Two Dimensional Time Dependent Incompressible Navier-Stokes Equations: High Reynolds Number Flows

John W. Goodrich
Lewis Research Center
Cleveland, Ohio

Prepared for the
Seventh International Conference on Numerical Methods in Laminar and Turbulent Flow
cosponsored by the Lockheed Missile & Space Company, Inc., Stanford University, Department of Chemical Engineering, International Journal for Numerical Methods in Fluids, and International Journal for Computational Methods in Heat and Fluid Flow
Stanford, California, July 15-19, 1991

NASA

An Efficient And Robust Algorithm For Two Dimensional Time Dependent Incompressible Navier-Stokes Equations: High Reynolds Number Flows

John W. Goodrich
National Aeronautics and Space Administration
Lewis Research Center
Cleveland, Ohio 44135

Abstract

An algorithm is presented for unsteady two dimensional incompressible Navier-Stokes calculations. This algorithm is based on the fourth order Partial Differential Equation for incompressible fluid flow which uses the streamfunction as the only dependent variable. The algorithm is second order accurate in both time and space, it uses a multigrid solver at each time step, it is extremely efficient with respect to use of both CPU time and physical memory, and it is extremely robust with respect to Reynolds number.

1. SUMMARY

An algorithm is presented for unsteady two dimensional incompressible Navier-Stokes calculations. This algorithm is based on the fourth order Partial Differential Equation for incompressible fluid flow which uses the streamfunction as the only dependent variable. The vorticity does not enter into this formulation. The algorithm is second order accurate in both time and space, it uses a multigrid solver at each time step, and it is extremely efficient with respect to use of both CPU time and physical memory. The algorithm is extremely robust with respect to Reynolds number, and has been used to directly compute incompressible flows with smoothly resolved streamfunction, kinetic energy and vorticity contours for Reynolds numbers as high as $Re = 100,000$ without requiring any subscale modelling. Solutions are shown for cavity flows at various Reynolds numbers.

2. THE ALGORITHM

In a bounded open region $\Omega \subseteq \mathbf{R}^2$, if ψ is the streamfunction, then the equation for two dimensional time dependent viscous incompressible flows with no body force can be written as

$$\frac{\partial \triangle \psi}{\partial t} + \frac{\partial \psi}{\partial y}\triangle\frac{\partial \psi}{\partial x} - \frac{\partial \psi}{\partial x}\triangle\frac{\partial \psi}{\partial y} - \frac{1}{Re}\triangle^2\psi = 0, \tag{1}$$

for x in Ω, and $t > 0$. Notice that this is a single equation for a single scalar unknown, and that neither vorticity nor pressure enter into the formulation. The velocity solution is obtained as

$$u(\mathbf{x},t) = \frac{\partial \psi}{\partial y}, \text{ and } v(\mathbf{x},t) = -\frac{\partial \psi}{\partial x}, \tag{2}$$

and it is always divergence free. One of the advantageous features of this formulation is that the scalar unknown ψ is smoother than the velocity and the vorticity, since they are both obtained from the streamfunction by differentiation. The data for the problem in this formulation consists of the initial data for ψ, and boundary data such as the standard set of boundary conditions

$$\psi(x,t) = \beta(x,t), \text{ and } \frac{\partial \psi}{\partial \eta}(x,t) = \gamma(x,t), \tag{3}$$

for x in $\partial\Omega$, and $t > 0$, where $\frac{\partial}{\partial \eta}$ is differentiation in the exterior normal direction at the boundary. A steady state form of Equation (1) was previouosly used by Schreiber and Keller [7] with path continuation methods for calculating high Reynolds number steady cavity flows.

Let $\tilde{\mathbf{z}}^n$ be the discrete grid function approximating ψ at time t_n. Using centered spatial differencing throughout, let La approximate the laplacian, let Bi approximate the biharmonic operator, and if

$$\mathrm{Cv}(\tilde{\mathbf{z}}^m)_{i,j} = \delta_x\Big(\delta_y(\tilde{\mathbf{z}}^m)\mathrm{La}(\tilde{\mathbf{z}}^m)\Big)_{i,j} - \delta_y\Big(\delta_x(\tilde{\mathbf{z}}^m)\mathrm{La}(\tilde{\mathbf{z}}^m)\Big)_{i,j}, \tag{4}$$

then let Cv approximate the convection terms. We discretize equation (1) as

$$\begin{aligned} &\mathrm{La}(\tilde{\mathbf{z}}^{n+1}) - \frac{\triangle t}{2Re}\mathrm{Bi}(\tilde{\mathbf{z}}^{n+1}) \\ &\qquad = \mathrm{La}(\tilde{\mathbf{z}}^{n}) + \frac{\triangle t}{2Re}\mathrm{Bi}(\tilde{\mathbf{z}}^{n}) - \frac{3\triangle t}{2}\mathrm{Cv}(\tilde{\mathbf{z}}^{n}) + \frac{\triangle t}{2}\mathrm{Cv}(\tilde{\mathbf{z}}^{n-1}). \end{aligned} \tag{5}$$

Notice that equation (5) for $\tilde{\mathbf{z}}^{n+1}$ is elliptic for all Reynolds numbers, and that it is linear with all of the nonlinearities lagged into the source term calculated from data at times t_n and t_{n-1}. The diffusion terms are time differenced with a Crank-Nicolson differencing scheme, which gives an infinite speed of propogation for the data at each time step through the elliptic biharmonic operator, and which does not impose a stability constraint on the time step size. The convection terms are time differenced with a lagged second order Adams-Bashforth differencing scheme, which does impose the CFL constraint $\frac{\|u\|\triangle t}{\triangle x} \leq 1$, where we assume that $\triangle x = \triangle y$. We have used a CFL number between 0.6 and 0.8 for calculations with Reynolds numbers between 100 and 100000, with grid sizes between $\frac{1}{32}$ and $\frac{1}{384}$. The local domain of dependance is the large symmetric 13 point discretization stencil from the discrete operators Bi and Cv. The velocity components $(u^n_{i,j}, v^n_{i,j})$ are directly recovered using (2) with centered differences, and are both defined at every grid point along with the streamfunction approximation $z^n_{i,j}$. The discrete velocity solution is exactly incompressible, since $\delta_x(u^n_{i,j}) + \delta_y(v^n_{i,j}) = 0$. This algorithm is related to a primitive variable method on a MAC staggered grid by the Finite Difference Galerkin Method (see Goodrich and Soh [5]).

When (5) is used as the finite difference approximation to (1), the problem that must be solved at each time step may be written as

$$\mathrm{La}(\tilde{\mathbf{z}}^{n+1}) - \frac{\triangle t}{2Re}\mathrm{Bi}(\tilde{\mathbf{z}}^{n+1}) = \tilde{\mathbf{f}}^{n,n-1}, \tag{6}$$

where $\tilde{\mathbf{f}}^{n,n-1}$ is the discrete source term from the right hand side of equation (5). We have used a banded LU decomposition solver to directly solve equation (6) by back substitution at every time step. In order to avoid the large storage overhead required by this approach, we currently use a multigrid method at each time step to solve equation (6). The multigrid solver factors Bi as two laplacians, it uses a Gauss Seidel or red black Gauss Seidel smoothing iteration, a linear restriction and prolongation, and a simple V cycle multigrid iteration using three smoothing sweeps while coarsening and none while refining. The factoring of Bi as two laplacians follows Linden [6], and introduces $\omega = \triangle\psi$ only for the purpose of having a convergent iteration scheme, but it incidentely produces both ψ and ω as simultaneeous solutions of a coupled Poisson and Laplace's equation. Note that $\tilde{\mathbf{f}}^{n,n-1}$ is always calculated from the right hand side of equation (5) using just the discrete streamfunction fields $\tilde{\mathbf{z}}^n$ and $\tilde{\mathbf{z}}^{n-1}$. Since $\omega = \triangle\psi$ is only introduced as an intermediate variable for solving equation (6) at each time step, its tendency toward a greater sensitivity to spatial disturbances and errors is not propagated to the solution ψ at subsequent time steps.

3. CAVITY CALCULATIONS

The examples for demonstrating the performance of this algorithm will be some typical two dimensional driven cavity calculations. For all driven cavity calculations, irrespective of Reynolds number and grid size, between 10 and 15 V cycles are used at each time step to reduce the residuals for equation (5) to less than 5×10^{-12}.

The performance of the algorithm will be shown by comparision of the calculation of a transient square driven cavity flow on an IBM RS/6000 model 530 workstation with three different uniform grids. The transient flow is the development from no initial flow with an impulsively started lid, from $t = 0$ to $t = 1$, with $Re = 9600$. The three calculations are: (a) with a 128×128 spatial grid, with 6 grid levels, and with $\triangle t = \frac{1}{160}$, requiring 1.7 MBytes of memory, and 2.5 CPU seconds per time step; (b) with a 192×192 spatial grid, with 7 grid levels, and with $\triangle t = \frac{1}{256}$, requiring 3.8 MBytes of memory, and 5.5 CPU seconds per time step; and (c) with a 256×256 spatial grid, with 7 grid levels, and with $\triangle t = \frac{1}{400}$, requiring 6.6 MBytes of memory, and 10.2 CPU seconds per time step. Notice first that the CPU time per time step increases linearly with the number of grid points. Simulation case (a) requires 1.50×10^{-4} seconds per time step per grid point, case (b) requires 1.48×10^{-4} seconds per time step per grid point, and case (c) requires 1.54×10^{-4} seconds per time step per grid point. The computional requirement for refined grids is not increased for each grid point for each time step, but the CFL constraint will require a time step size that decreases linearly with the spatial grid size for the refined grid, so that more time steps are required for the same nondimensional time interval. If the additional time steps that are required for the entire calculation from $t = 0$ to $t = 1$ are considered as part of the computational cost, then refining the grid from a 128×128 to a 192×192 grid actually requires 1.6 times more CPU time per grid point for the entire calculation on the finer grid, and refining again from a 192×192 to a 256×256 grid also requires 1.6 times more CPU time per grid point for the entire calculation. Notice also that the memory requirement increases linearly with the number of grid points. Simulation case (a) requires 107.12 Bytes per grid point, case (b) requires 106.97 Bytes per grid point, and case (c) requires 104.78 Bytes per grid point. The observed linear increase in CPU and memory requirements with an increase in the number of grid points is typical of multigrid solvers, since it is well known that the order of computational effort for these solvers is $O(N)$, where N is the total number of grid points.

The accuracy of the algorithm will be shown by comparing sample results for the driven cavity with established results in the literature by Ghia et.al. [1]. Figure (1) presents driven cavity results with a 256×256 grid for $Re = 5000$. This data was calculated using the time dependent algorithm presented above with $\triangle t = \frac{1}{400}$, and is for the state of the flow at $t = 748.45$ when the time evolution has virtually stopped. The cavity has its upper lid moving from the left to the right, and all three of its other walls are not moving. The length scale is such that the cavity walls have length 1, and the velocity and time scales are established by using 1 as the lid velocity. The streamfunction contours in Figure (1a) show the usual assortment of primary and secondary circulation patterns, but the contours

do not show tertiary circulations that are actually resolved in the lower two corners. The tertiary recirculating eddy in the lower right hand corner is resolved by 14×11 grid points, while the smaller tertiary eddy hidden below the streamfunction contours in the lower left hand corner is resolved by only 4×3 grid points. Figure (1b) shows the vertical velocity component in a horizontal crossection across the middle of the cavity. The calculated data is compared with the data in Ghia, et.al. [1], and shows complete agreement with the published data. Figure (1c) shows the horizontal velocity component in a vertical crossection up the middle of the cavity, and Figure (1d) shows the vorticity on the upper lid. This data also shows complete agreement with the published data. The acurracy of the computed solution is also shown by quantitative comparisons between the calculated and published data for the values and locations of the streamfunction minimum and maximum. The global streamfunction minimum occurs in the center of the primary circulation, and the global streamfunction maximum occurs in the center of the lower right hand secondary corner eddy. This data is given in Table 1, along with established data from a calculation on a 256×256 grid published in Ghia, et.al. [1]. There is excellant agreement between our solution and the published data in Ghia, et.al. [1], where both calculations are on a 256×256 grid. Our calculated solution on a 128×128 grid also shows very good agreement with the published data on a 256×256 grid.

The degree of agreement between our calculated results and the published data for the driven cavity at $Re = 5000$ is also characteristic of our calculations at $Re = 7500$. For $Re = 10000$ (Goodrich [2]), our calculated results differ dramatically from the published steady state solutions for the driven cavity. Instead of converging to a steady state, our time dependent calculations show convergence to an unsteady time asymptotic state. In fact, our calculations (Goodrich [3]) show a steady state for $Re = 8900$, and periodic time asymptotic solutions with spectra that have a single fundamental frequency for $Re = 9000$, $Re = 9500$ and $Re = 9600$. All three of these time asymptotic flows with single fundamental frequencies have been calculated on 128×128 grids with $\triangle t = \frac{1}{160}$. The periodic flow for $Re = 9600$ has a fundamental frequency of 0.55 ± 0.005 on a 128×128 grid. A second calculation at $Re = 9600$ was done on a 192×192 grid with $\triangle t = \frac{1}{256}$, and this calculation also produced a periodic time asymptotic flow with one fundamental frequency of 0.58 ± 0.005. The data for $3600 < t \leq 3700$ from this calculation on the 192×192 grid is presented in Figure (2a) as a phase portrait of ψ_{min} on the vertical axis versus the total kinetic energy on the horizontal axis. This data is for 100 nondimensional time units, or for 25600 discrete time steps, and for approximately 58 complete periodic cycles of the time asymptotic flow. The period of the asymptotic flow state is 1.72 ± 0.015, so that each cycle requires approximately 440 discrete time steps. Notice the fact that the oval plot appears to be a single line. This exact repetition of the phase portrait through 58 cycles shows the precise periodicity of the asymptotic state. The qualitative and quantitative agreement of the dynamics from these two calculations on separate grids supports the grid independence of the periodic time asymptotic solution in the driven cavity at $Re = 9600$. For higher Reynolds numbers we find more complex dynamics. At $Re = 9700$ on a 128×128 grid we find two incomensurate fundamental frequencies, and the unsteady time asymptotic solution is aperiodic with a discrete spectrum. A phase portrait for this flow is given in

Figure (2b), which shows a plot of ψ_{min} on the vertical axis versus the total kinetic energy on the horizontal axis for $3700 < t \leq 4500$. The data plotted in Figure (2b) is for 800 nondimensional time units, or for 128600 discrete time steps, and it qualitatively shows the dramatically more complex yet highly structered aperiodic time asymptotic state at $Re = 9700$. At $Re = 10000$ on a 128×128 grid, we also find two incomensurate fundamental frequencies, and this unsteady time asymptotic solution is also aperiodic with a discrete spectrum (see Goodrich [2]). These solutions suggest a first Hopf bifurcation in the square driven cavity for $8900 < Re < 9000$, and a second one for $9600 < Re < 9700$.

It could very well be argued that all of these unsteady time asymptotic solutions in the driven cavity are spurious, since there are established steady solutions for $Re = 10000$. On the other hand, the most well known of these solutions (Ghia, et.al. [1], Schreiber and Keller [7]) use steady state methods, and unsteady time dependent methods for high Reynolds number flows tend to introduce artifical dissipation, which we have avoided. Furthermore, Shen [8] has used a Chebychev Tau method to detect a Hopf bifurcation in the regularized driven cavity for $10000 < Re < 10500$. The use of a spectral method with similar results lends plausibility to our claims, since the parabolic velocity profile for the regularized cavity lid should transmit less momentum to the cavity interior, and the transition to unsteady time asymptotic states could reasonably be expected to occur at a higher Reynolds number. There are also periodic solutions in the aspect two rectangular driven cavity using our algorithm (Goodrich, et.al. [4]) which show the same generic behavior in a deeper cavity and at a lower Reynolds number. Unsteady time asymptotic flows are completly consistent with what should be expected in light of the current understanding of nonlinear dynamical systems (see [9]). It is possible that our algorithm has dispersion or other error characterisitcs that prematurely trigger a Hopf bifurcation at too low a Reynolds number, but the cumulative effect of the considerations introduced above is that the transition to unsteady time asymptotic states such as we have observed should be expected, and that the critical Reynolds numbers for the transitions that we have observed are plausible.

The robustness of the algorithm with respect to Reynolds number will be shown by data from a direct computation of a transient square cavity flow with an impulsively started lid on a 256×256 uniform grid at $Re = 25000$. Figures (3a-b) show streamfunction and vorticity contours at $t = 10.25$, early in the transient flow development from the initial state of rest. The vorticity plot clearly shows a large number of small structures that are being created in the boundary layer beneath the wall jet, which is descending from the end of the moving lid, and which is separating from the right hand wall. This series of small scale structures is ejected from the boundary layer and convected around the large central recirculation pattern, to appear either as small recirculating eddies or as waves all around the central structure in the cavity. Notice in the vorticity plot that the series of small scale structures is wrapped around and folded back into the central structure, resulting in a twisted or spiral shaped composite structure that has multiple layers like a fine pastry. Figures (3c-d) show streamfunction and vorticity contours at $t = 83$, and Figures (3e-f) show streamfunction and vorticity contours at $t = 84$. These plots show the state of the

flow after sufficient time has elapsed for the development of all the usual secondary flow structures in the cavity. In addition to these secondary structures, we also observe a very active collection of tertiary flow structures, that originate in the boundaries and corners of the cavity, that are convected and distorted by the local flow while interacting with the primary, secondary and tertiary structures, and that ultimately either dissipate or combine with other structures. As an example, consider the tertiary eddy that is rising along the middle of the left hand wall at $t = 84$. This structure can be seen at $t = 83$ as the small tertiary structure that is just beginning to pull out of the recirculation complex in the lower left hand corner. This tertiary eddy actually originated at about $t = 78$ in the lower right hand corner, and it then separated from that corner to be rolled along the lower wall, until it attached to and moved along the upper surface of the lower left hand corner complex. For $t > 84$, this tertiary structure will continue up the left hand wall until it attaches to and rolls along the surface of the secondary structure in the upper left near the lid, ultimately being absorbed by this secondary eddy. Besides the complexity of structures on several scales, at $t = 83$ and $t = 84$, we also observe that the vorticity in the center of the cavity is not uniform. We see a continuous elastic deformation of the primary circulation structure in the center of the cavity, which stretches and moves while it rotates. The observed flow clearly does not have a central core of uniformly rotating fluid with constant vorticity at $t \approx 83$. This computation has not yet been carried further than $t = 100$, so that we do not yet know how the asymptotic flow state can be characterised at $Re = 25000$. The issue of whether or not the 256×256 grid is adequate for resolving the relevant length scales at $Re = 25000$ is also not answered by this single transient calculation. Nevertheless, we do observe that the streamfunction and vorticity fields are smoothly resolved by our algorithm at $Re = 25000$ with a 256×256 grid, and this clearly shows the robustness of our algorithm with respect to Reynolds number.

Bibliography

[1] U. Ghia, K. N. Ghia and C. T. Shin, *J. Comput. Phys.* **48** , 387 (1982).

[2] J. W. Goodrich, "An Unsteady Time Asymptotic Flow in the Square Driven Cavity," in *Proc. IMACS* 1st *Intern. Conf. on Comput. Phys.*, Ed: K. Gustafson and W. Wyss, (Univ. of Col. at Boulder, June 1990), and as NASA TM 103141.

[3] J. W. Goodrich, in preparation.

[4] J. W. Goodrich, K. Gustafson and K. Halasi, *J. Comput. Phys.* **90** , 219 (1990), and as ICOMP Report 89-21, NASA Lewis R. C., Cleveland, OH (1989).

[5] J. W. Goodrich and W. Y.Soh, *J. Comput. Phys.* **84** , 207 (1989).

[6] J. Linden, "A Multigrid Method for Solving the Biharmonic Equation on Rectangular Domains," Arbeitspapiere der GMD No. 143, Gesellschaft für Mathematik und Datenverarbeitung, St. Augustin, (1985).

[7] R. Schreiber and H. B. Keller, *J. Comput. Phys.* **49**, 310 (1983).

[8] J. Shen, "Hopf Bifurcation of the Unsteady Regularized Driven Cavity Flows," Report No. 8906, The Inst. for Applied Math. and Sc. Compt., Indiana University, Bloomington, IN (April 1989).

[9] R. Temam, *Infinite-Dimensional Dynamical Systems in Mechanics and Physics*, (Springer-Verlag, New York, 1988).

The Streamfunction Minimum

Source	Grid	ψ_{min}	x_{min}	y_{min}
Goodrich	128×128	-1.15×10^{-1}	$\frac{66}{128} = \frac{132}{256}$	$\frac{69}{128} = \frac{138}{256}$
Goodrich	256×256	-1.18×10^{-1}	$\frac{132}{256}$	$\frac{137}{256}$
Ghia, et.al.	256×256	-1.19×10^{-1}	$\frac{131}{256}$	$\frac{137}{256}$

The Streamfunction Maximum

Source	Grid	ψ_{min}	x_{min}	y_{min}
Goodrich	128×128	3.44×10^{-3}	$\frac{102}{128} = \frac{204}{256}$	$\frac{9}{128} = \frac{18}{256}$
Goodrich	256×256	3.13×10^{-3}	$\frac{206}{256}$	$\frac{19}{256}$
Ghia, et.al.	256×256	3.08×10^{-3}	$\frac{207}{256}$	$\frac{19}{256}$

Table 1: STREAMFUNCTION MAX AND MIN
The square driven cavity at Re=5000

Figure 1: $Re = 5000$, 256×256 grid, $\Delta t = \frac{1}{400}$, $t = 748.45$,
calculated data compared with Ghia, et.al.

1a: Stream Function Contours

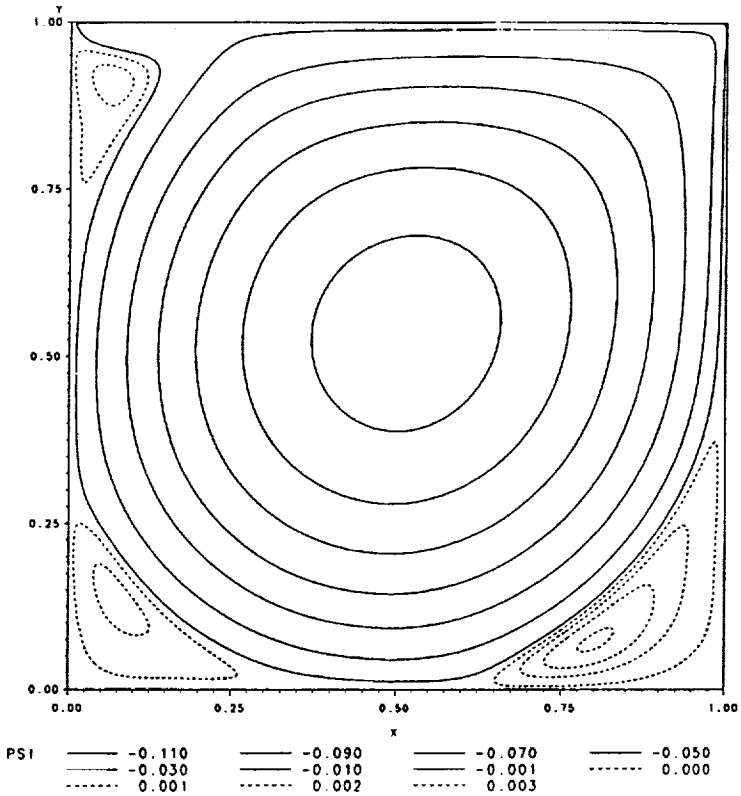

1b: v at y=0.5

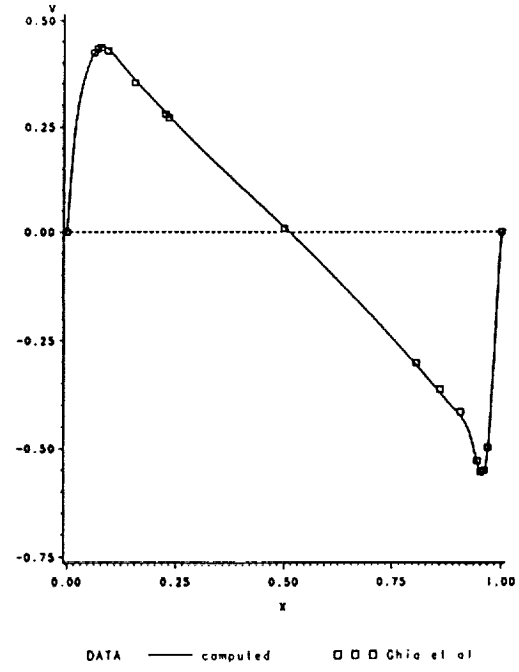

1c: u at x=0.5

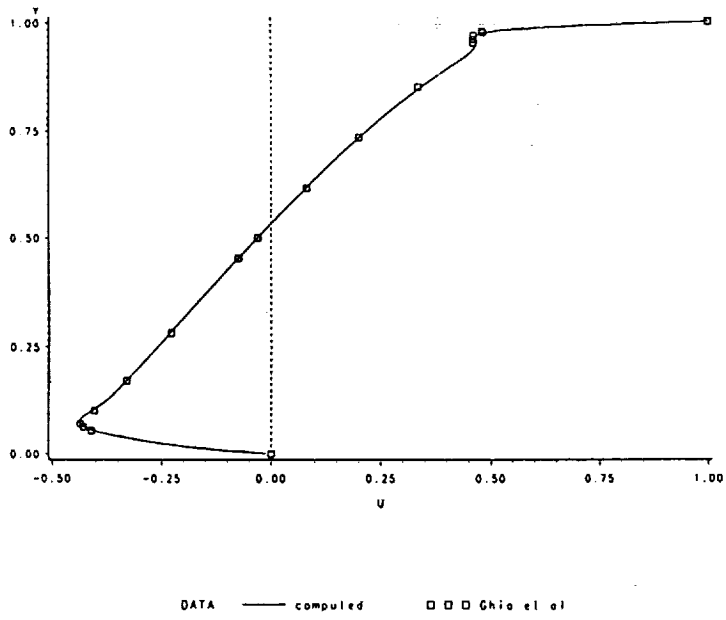

1d: Vorticity at y=1

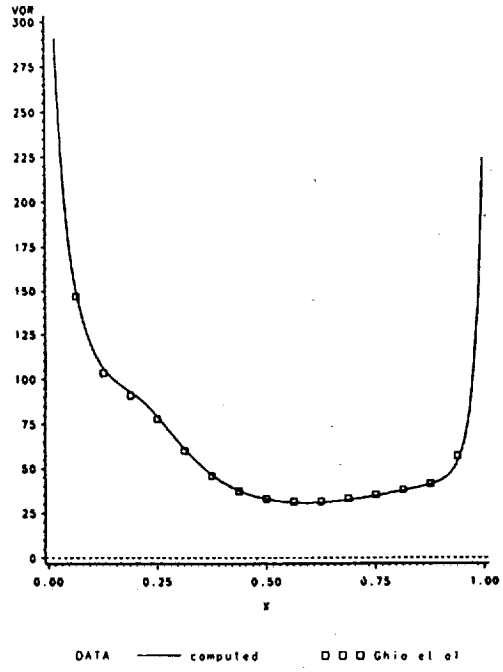

Figure 2: Phase Portraits of ψ_{min} versus Total Kinetic Energy

2a: $Re = 9600$,
192×192 grid,
$3600 < t \leq 3700$

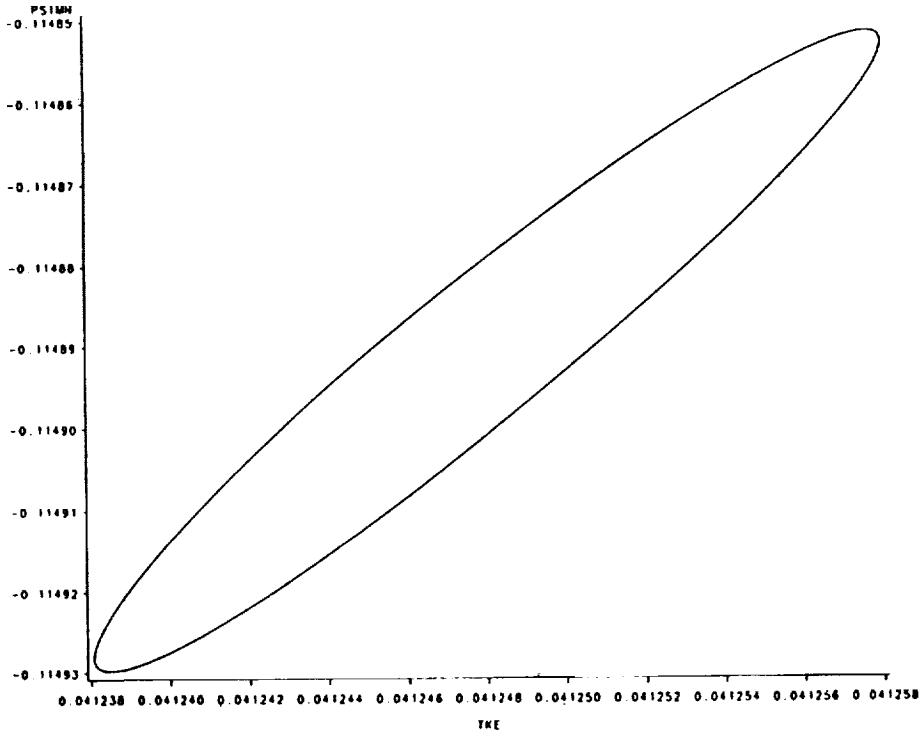

2b: $Re = 9700$,
128×128 grid,
$3700 < t \leq 4500$

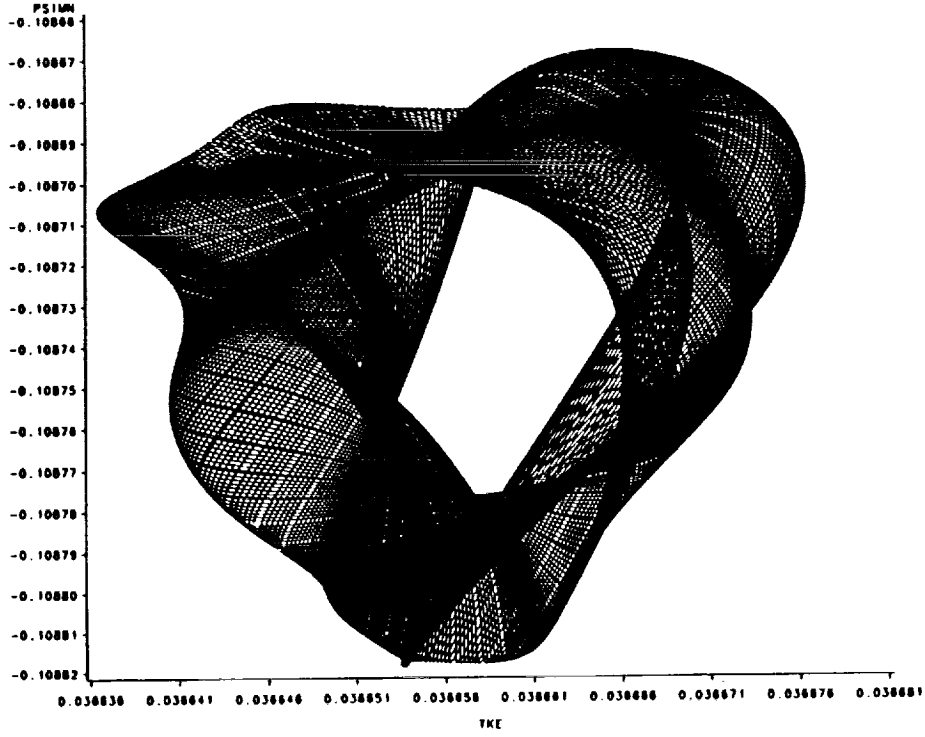

Figure 3: $Re = 25000$, 256×256 grid, $\Delta t = \frac{1}{400}$, transient calculation.

3a: Streamfunction Contours, t=10.25

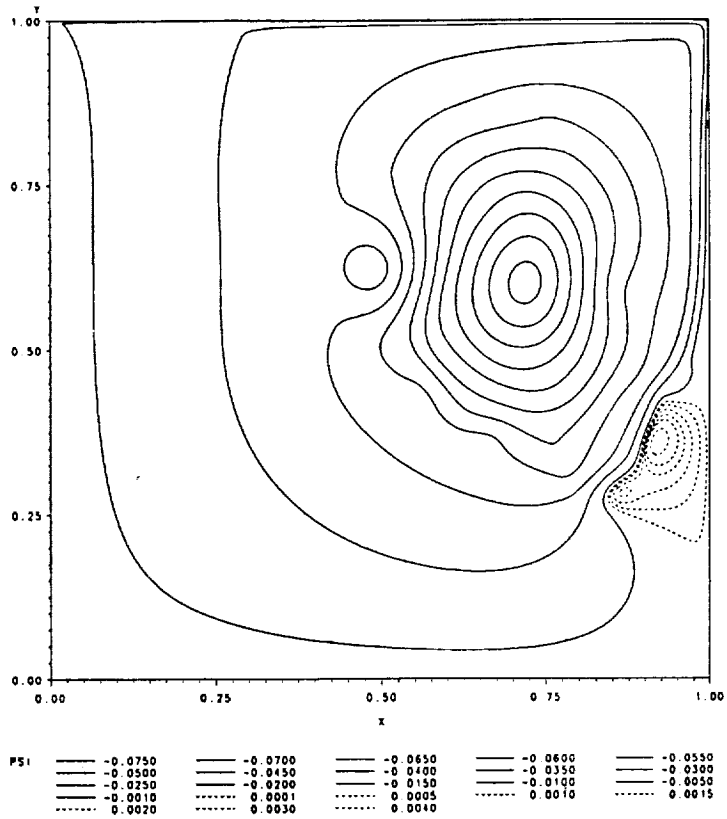

3b: Vorticity Contours, t=10.25

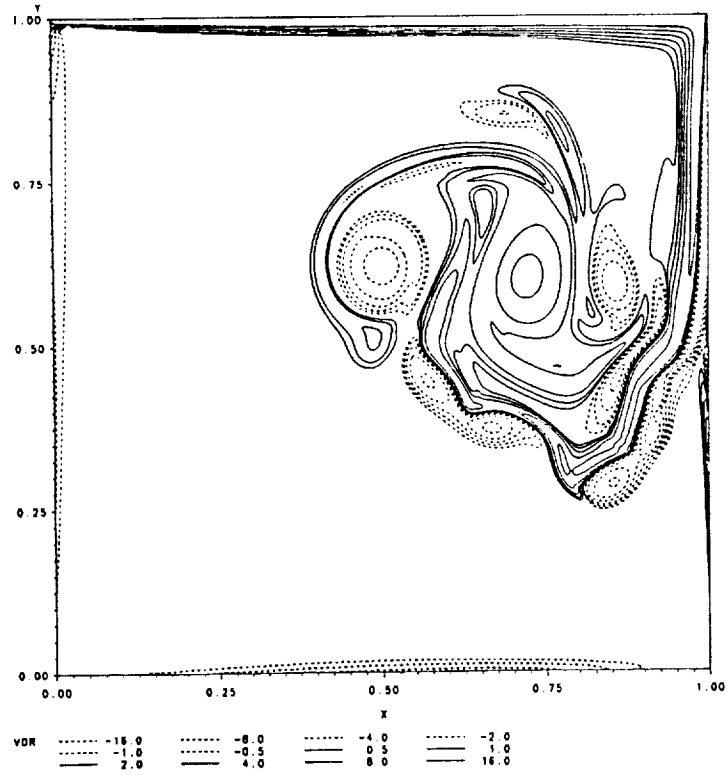

3c: Streamfunction Contours, t=83

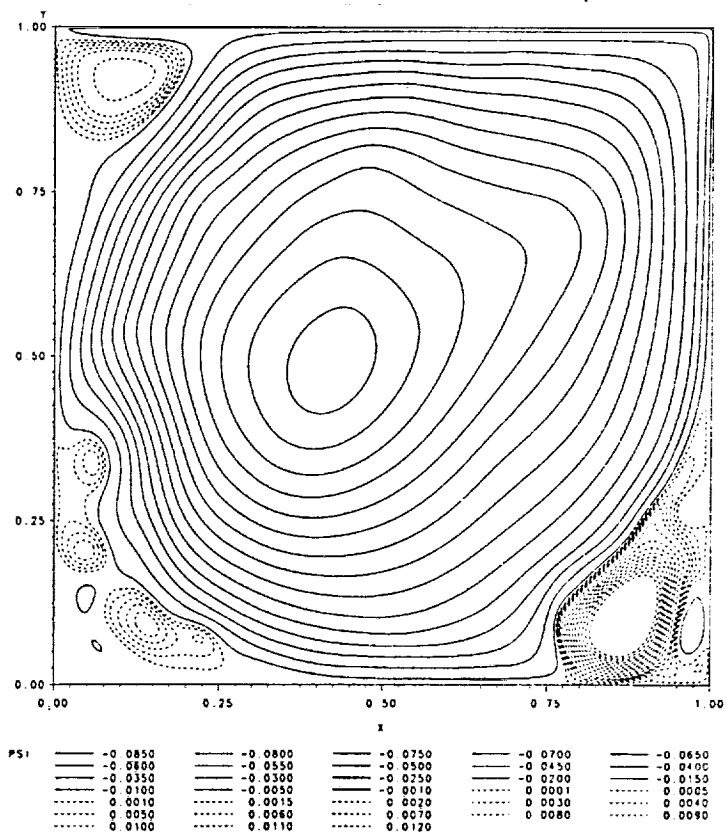

3d: Vorticity Contours, t=83

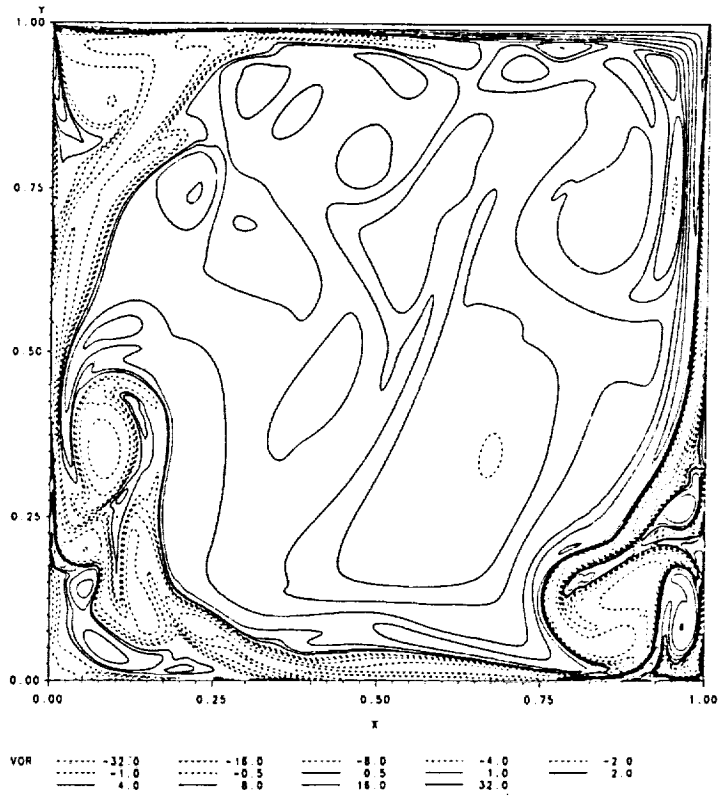

3e: Streamfunction Contours, t=84

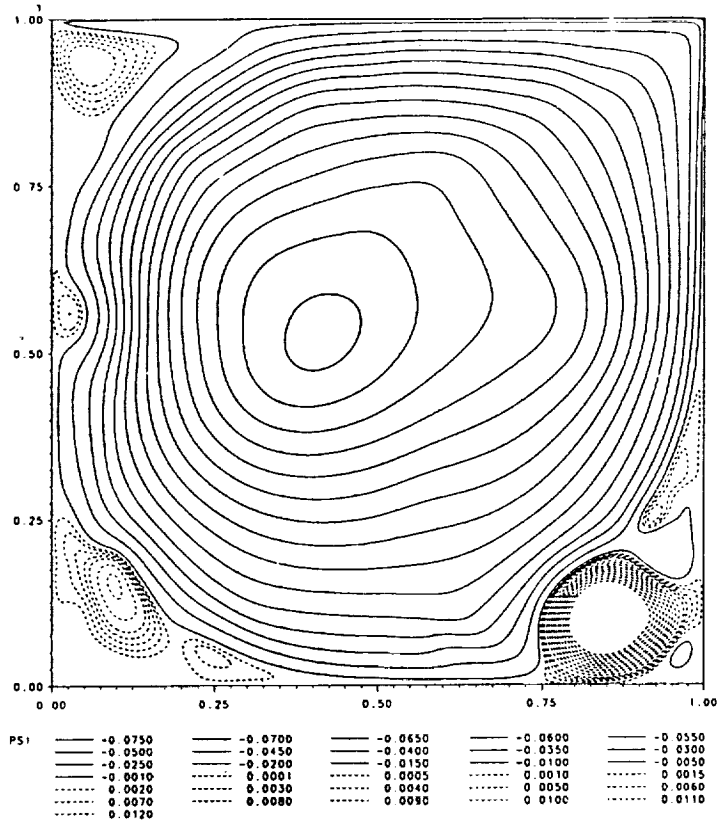

3f: Vorticity Contours, t=84

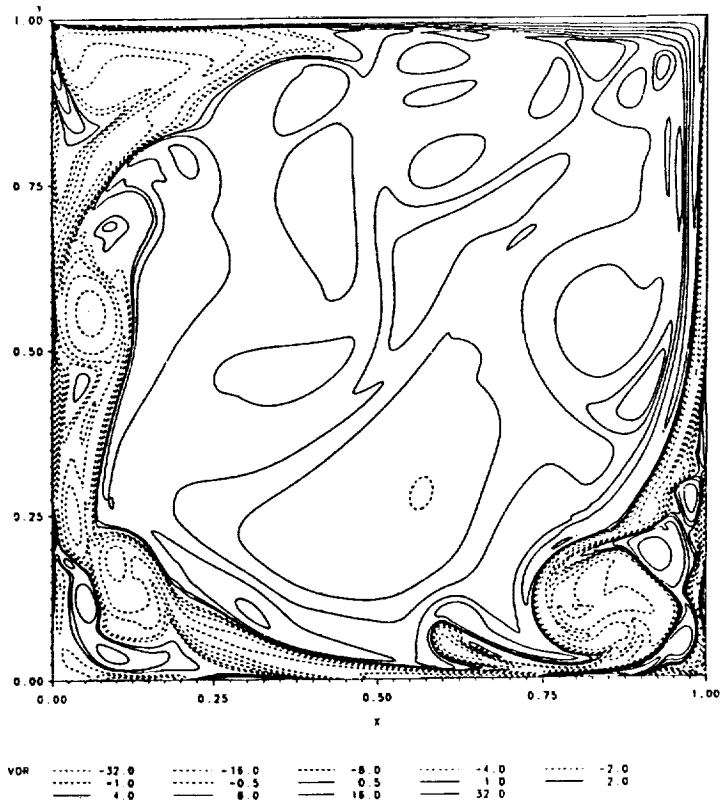

NASA
National Aeronautics and Space Administration

Report Documentation Page

1. Report No.	2. Government Accession No.	3. Recipient's Catalog No.
NASA TM -104424		

4. Title and Subtitle
An Efficient and Robust Alogrithm for Two Dimensional Time Dependent Incompressible Navier-Stokes Equations: High Reynolds Number Flows

5. Report Date

6. Performing Organization Code

7. Author(s)
John W. Goodrich

8. Performing Organization Report No.
E -6257

10. Work Unit No.
505 -62-21

9. Performing Organization Name and Address
National Aeronautics and Space Administration
Lewis Research Center
Cleveland, Ohio 44135 - 3191

11. Contract or Grant No.

13. Type of Report and Period Covered
Technical Memorandum

12. Sponsoring Agency Name and Address
National Aeronautics and Space Administration
Washington, D.C. 20546 - 0001

14. Sponsoring Agency Code

15. Supplementary Notes
Prepared for the Seventh International Conference on Numerical Methods in Laminar and Turbulent Flow cosponsored by Lockheed Missile & Space Company, Inc., Stanford University, Department of Chemical Engineering, International Journal for Numerical Methods in Fluids, and International Journal for Computational Methods in Heat and Fluid Flow, Stanford, California, July 15-19, 1991. Responsible person, John W. Goodrich, (216)433-5922.

16. Abstract
An algorithm is presented for unsteady two dimensional incompressible Navier-Stokes calculations. This algorithm is based on the fourth order Partial Differential Equation for incompressible fluid flow which uses the streamfunction as the only dependent variable. The algorithm is second order accurate in both time and space, it uses a multigrid solver at each time step, it is extremely efficient with respect to use of both CPU time and physical memory, and it is extremely robust with respect to Reynolds number.

17. Key Words (Suggested by Author(s))	18. Distribution Statement
Time dependence; Incompressibility; Navier-Stokes equation; High reynolds number; Flow; Alorithms	Unclassified - Unlimited Subject Category 34

19. Security Classif. (of the report)	20. Security Classif. (of this page)	21. No. of pages	22. Price*
Unclassified	Unclassified	16	A03

NASA FORM 1626 OCT 86

*For sale by the National Technical Information Service, Springfield, Virginia 22161